Letter

Vol. 50, No. 7 / 1 April 2025 / *Optics Letters* 2449

Optics Letters

Dispersive eye-box extension in micro-OLED augmented reality glasses with a dual-holographic dispersion-compensating reflective combiner

Sangyoon Kim,[1] Hosung Jeon,[2] Youngjin Jeon,[1] Youngsub Kim,[1] Joonku Hahn,[2] and Hwi Kim[1,*]

[1] *Department of Electronics and Information Engineering, College of Science and Technology, Korea University, Sejong-Campus, 2511 Sejong-ro, Sejong 30019, Republic of Korea*

[2] *School of Electronic and Information Engineering, Kyungpook National University, 80 Daehak-ro, Buk-Gu, Daegu 41566, Republic of Korea*

**hwikim@korea.ac.kr*

Received 17 January 2025; revised 19 February 2025; accepted 1 March 2025; posted 10 March 2025; published 1 April 2025

We propose an eye-box extension method for augmented reality (AR) glasses utilizing a dual-holographic optical element (dual-HOE) and a micro-OLED (µOLED) light source with a broadband spectrum. This scheme leverages the strong chromatic dispersion of HOE to significantly extend the eye-box without compromising AR quality. The proportional relationship between µOLED spectral bandwidth and eye-box size is analyzed theoretically, indicating that a broader spectrum µOLED provides a wider eye-box. Experimental results using a prototype demonstrate eye-box expansion up to 8 mm for µOLED with a 60 nm spectral bandwidth.

https://doi.org/10.1364/OL.555710

The rapid adoption of augmented reality (AR) technologies has accelerated the development of lightweight and compact AR near-eye displays (NEDs) [1]. Among these, off-axis reflection-type holographic optical element (HOE) combiners have garnered attention for their simplicity and the form factor that resembles traditional, user-friendly eyeglasses [2]. However, challenges such as limited field of view (FOV), small eye-box, and chromatic dispersion persist in the reflection-type HOE AR-NEDs, which are caused by the wavelength and angular selectivity of the HOE [3,4]. The wavelength selectivity of HOEs causes chromatic dispersion aberrations, resulting in image distortion and reduced clarity [5,6]. Additionally, the angular selectivity of HOEs restricts diffraction efficiency for wide-angle incoming light, further limiting the FOV [7]. A particularly significant issue is the small eye-box, which makes the HOE AR-NED impractical as image perception is highly sensitive to the viewer's eye movements [8]. Conventional approaches often employ monochromatic laser sources precisely matched to the HOE's recording wavelength [9,10]. While effective in minimizing chromatic dispersion, these laser sources inherently introduce speckle noise, significantly degrading image quality and visual comfort [11]. To address these challenges, recent advancements emphasize the adoption of self-emissive incoherent displays such as micro-OLED (µOLED) or micro-LED, which reduce or eliminate speckle noise [12]. Commercial µOLEDs emerge as a promising alternative for reflection-type HOE AR-NED, offering partial coherence or incoherence to suppress speckle noise. However, the accompanying spectral broadening exacerbates chromatic dispersion, leading to AR image blurring. Moreover, the small eye-box remains a critical issue requiring resolution.

In this Letter, we propose a novel dual-HOE configuration integrated with µOLED displays to address the challenges of chromatic dispersion and a narrow eye-box simultaneously. The proposed dual-HOE system effectively extends the eye-box without compromising the FOV or image quality. Figure 1(a) presents the prototype of the proposed AR-NED, which incorporates a dual-holographic dispersion-compensating reflective combiner and a µOLED projector. Designed as the form of everyday eyewear, the prototype features an eye-relief (the distance between the glasses and the viewer's eye) fixed at 20 mm. The system consists of four main components: a transmissive HOE (H_T), a reflective HOE (H_R), a projection optics, and a µOLED panel with an emission spectrum of 60 nm bandwidth centered at a wavelength of 620 nm (Fig. 1(b)). H_T and H_R are complementary one-dimensional holographic linear volume gratings. The parallel setting of H_T and H_R comprises the dual-HOE configuration (Fig. 1(d)), where light emitted from the µOLED is deflected by H_T with strong chromatic dispersion and subsequently reflected by H_R with the dispersion compensated (Fig. 1(d)). As a result, broadband light from the µOLED propagates through the dual-HOE without chromatic dispersion. In order to clearly understand the effect of dispersion on the perceived AR image, the dual-HOE AR-NED system in Fig. 1(d) is compared with the single-HOE AR-NED system, which lacks a dispersion compensation mechanism. In the single-HOE system illustrated in Fig. 1(c), the AR image exhibits blurring caused by the strong chromatic dispersion of H_R. In contrast, a deblurred, clean AR image is observed in the dual-HOE system as shown in Fig. 1(d). The dispersion compensation mechanism will be analyzed in detail in Fig. 3. As illustrated in the schematic diagram in

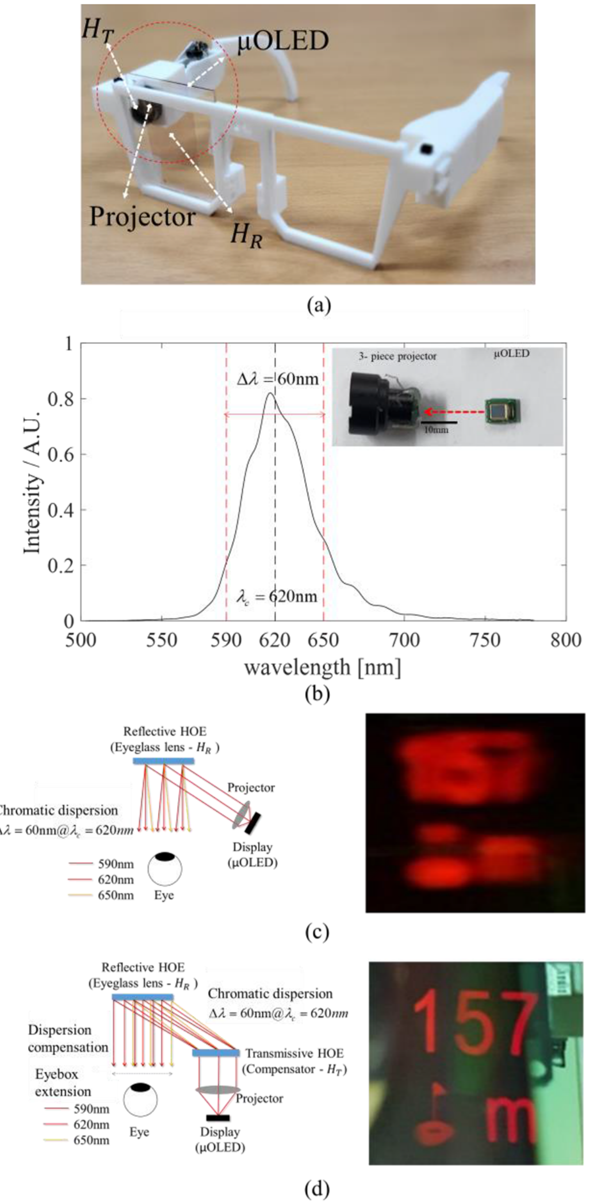

Fig. 1. (a) Prototype of the proposed dual-HOE AR-NED and (b) emission spectrum of the μOLED with 60 nm bandwidth ranging from λ = 590 nm to λ = 650 nm at the center wavelength of 620 nm. (c) Single-HOE AR-NED producing a blurred image due to chromatic dispersion and (d) dual-HOE AR-NED showing a dispersion-compensated AR image.

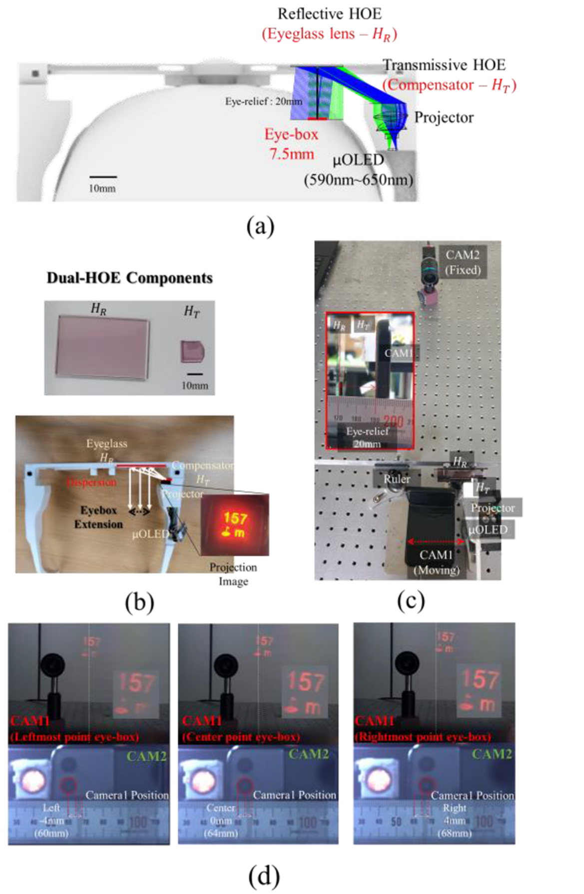

Fig. 2. (a) ZEMAX ray tracing of the dual-HOE AR-NED prototype, (b) the dual-HOE components and the AR-NED prototype, (c) measurement setup of the eye-box, and (d) AR image observation at the leftmost point, the center, and the rightmost point within the eye-box (see Visualization 1).

Fig. 1(d), the dual-HOE configuration with a broadband μOLED demonstrates a distinct advantage in effective eye-box extension compared to configurations using monochromatic light sources.

To evaluate the eye-box extension effect of the proposed scheme, we conduct ZEMAX modeling of the prototype and estimate the eye-box size of the AR-NED, as shown in Fig. 2(a). The prototype design utilizes a μOLED emission spectrum of $\Delta\lambda = 60$ nm ranging from 590 nm to 650 nm. The display module is integrated into the temples of the glasses, and the dispersion compensation HOE, H_T, is designed with the 1st order diffraction angle of 56° for normal incidence, preventing the diffracted light from interfering with the viewer's face. In the ray tracing simulation, light emitted from the leftmost pixel of the μOLED reaches the viewer's eye as an infinitely collimated ray bundle, colored green, after collimation through the projector optics and passing through the dual-HOE system. The horizontal incidence angle of the ray bundle is estimated at −3.06° relative to the vertical axis. The light emitted from the rightmost pixel of the μOLED, colored blue, reaches the viewer's eye at an angle of 3.06°. This analysis defines the lateral size of the eye-box as the geometric overlap area between the rays from the leftmost and rightmost pixels on the eye plane. For the prototype, the horizontal eye-box size is estimated at 7.5 mm. Furthermore, the analysis reveals a diagonal FOV of 8°, which includes a horizontal FOV of 6.12° spanning from −3.06° to 3.06° and a vertical FOV of 5.15° spanning from −2.575° and 2.575°. During the design process, the trade-off between FOV and eye-box was carefully considered, adhering to compact form factor guidelines suitable for everyday eyewear.

Figure 2(b) shows the top-view of the AR-NED prototype and its key components, including the HOE parts, H_T and H_R. The base material for H_T and H_R is a holographic photopolymer film with a thickness of 16 μm (manufactured by Liti Holographics Inc.). The projector is a custom-designed collimating optical system composed of three aspheric lenses. Both H_T and H_R are planar, one-dimensional holographic volume gratings compactly cut to fit into the temple of the glasses and placed in parallel. An experiment was conducted to measure the eye-box and validate the prototype design. Figure 2(c) presents the experimental setup, which includes two cameras: CAM1, mounted on a linear stage and acting as the viewer's eye to observe augmented reality (AR) images, and CAM2, which monitors the movement of the center of CAM1's aperture to determine the eye-box boundaries. In the experiment, the eye-box is defined as the area within which a viewer's eye can perceive the entire AR image from the μOLED display without clipping. The FOV is determined by the maximum AR image size observed at the center of the eye-box. Figure 2(d) presents the AR images captured by CAM1 at three specific positions: the leftmost point, the center, and the rightmost point of the eye-box. The leftmost point represents the eye-box's left boundary, where CAM1 can view the complete AR image with an 8° FOV without any image information loss. Similarly, the right boundary of the eye-box is determined by the measurement of the rightmost point where CAM1 can fully perceive the AR image. The total distance traveled by CAM1 from the leftmost point to the rightmost point is measured to be 8 mm, which is the experimental horizontal eye-box size of the prototype at 20 mm eye-relief. The experimentally measured horizontal eye-box of 8 mm agrees well with the numerically estimated horizontal eye-box of 7.5 mm. The eye-box is actually very sensitive to variations in the eye-relief distance. While the design specifies that a 20 mm eye-relief corresponds to 7.5 mm eye-box, experimental deviation in eye-relief can alter the eye-box size up to ±0.5 mm. Shorter eye-relief distances can slightly extend the eye-box, while longer distances reduce it. These results underscore the consistency between the ZEMAX simulation model and the fabricated prototype.

Comparative K-diagram analysis in Fig. 3 elucidates the relationship between dispersion compensation and eye-box extension in the dual-HOE system. Figures 3(a) and 3(b) depict the eye-box extent for systems utilizing μOLEDs with narrowband ($\Delta\lambda = 20$ nm) and broadband ($\Delta\lambda = 60$ nm) emissions, respectively. Light emitted from μOLEDs with narrow and broad spectral bandwidths is collimated by the projector and passes through H_T. As the light traverses H_T, dispersion occurs by the grating vector $\vec{G}_T$. In the case of the μOLED with a broad spectral emission, the dispersion is significantly wider. The k-space analysis presented in the bottom panel presents that dispersed light emerging from H_T is subsequently collimated by H_R featured with the grating vector $\vec{G}_R$. During the recording process of the HOEs, H_T and H_R, precise alignment of the reference beam and signal beam is crucial to minimize errors in the generation of the grating vectors, $\vec{G}_T$ and $\vec{G}_R$. Greater dispersion results in a broader collimated illumination on the viewer's eye. By carefully adjusting the k-vectors of the dispersed light in two stages, the dual-HOE system achieves non-dispersed image quality over a wide spectral bandwidth, thereby extending the eye-box in proportion to the light's spectral bandwidth.

To further assess the dual-HOE configuration's eye-box extension according to the emission bandwidth of μOLED display, ZEMAX ray-tracing simulations are performed. As shown in Figs. 4(a)–4(d), the analysis highlights the eye-box variation with increasing the bandwidth of a light source from narrowband ($\Delta\lambda = 20$ nm) to broadband ($\Delta\lambda = 80$ nm). At $\Delta\lambda = 20$ nm, depicted in Fig. 4(a), insufficient overlap of the ray bundles from the leftmost and rightmost edge pixels of μOLED is observed, which prevents the formation of eye-box. When the spectral bandwidth is increased to 40 nm, as shown in Fig. 4(b), an

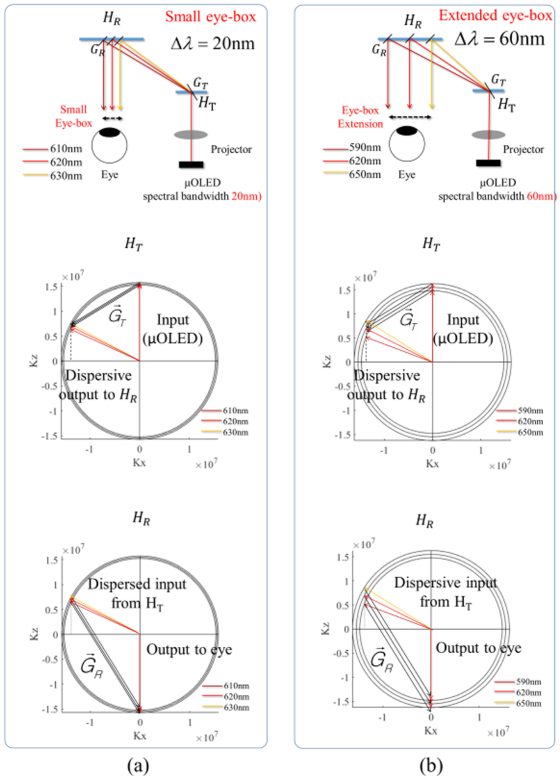

Fig. 3. Dispersive eye-box extension as a function of μOLED spectral bandwidth. (a) Small eye-box with $\Delta\lambda = 20$ nm narrowbandwith μOLED and (b) larger eye-box with $\Delta\lambda = 60$ nm broadbandwidth μOLED.

eye-box with a width of 3.4 mm is formed, fully encompassing the μOLED display area without clipping or vignetting. Further bandwidth increases to 60 nm and 80 nm presented in Figs. 4(c) and 4(d), respectively, result in proportional extension of the eye-box to 7.5 mm and 11.1 mm. These simulations indicate that substituting the current μOLED with the one possessing a broader spectral bandwidth can effectively and substantially enhance the horizontal eye-box.

Regarding the vertical eye-box, it remains unaffected by the absence of grating components. This design ensures structural stability, even when the μOLED's spectral bandwidth increases. ZEMAX simulations confirms that the vertical FOV remains constant at 5.15°, with the vertical eye-box size unchanged at 9.9 mm, irrespective of μOLED bandwidth.

The overall geometric design of the glasses influences the arrangement and performance of the optical components, affecting the FOV, eye-box size, and form factor. In the current dual-HOE system design, the vertical direction FOV and eye-box are independent of the HOE configuration, enabling alternative enhancements. These include the integration of cylindrical lenses recorded into HOE to enhance the vertical FOV. Additionally, employing established HOE techniques, such as angular multiplexing, offers the potential to simultaneously expand both the FOV and eye-box dimensions.

From a design perspective, as the diffraction angle of H_T increases, the position of H_T shifts closer to the surface of the glasses, directly influencing the eye-box size. For effective eye-box extension, the diffracted light must cover a wide area on H_R. However, a larger diffraction angle of H_T shortens the optical

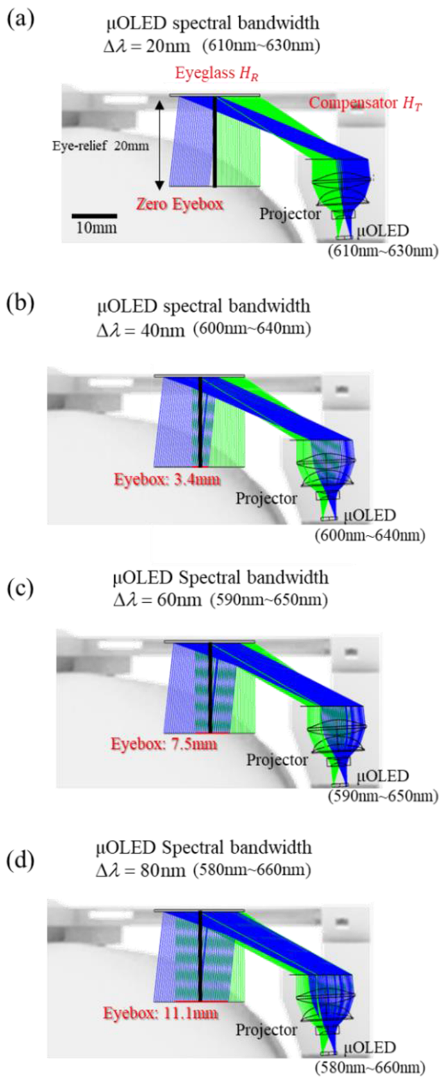

Fig. 4. Ray tracing simulation of eye-box changes for the variations in the spectral bandwidth of the μOLED: (a) $\Delta\lambda$ = 20 nm, (b) $\Delta\lambda$ = 40 nm, (c) $\Delta\lambda$ = 60 nm, and (d) $\Delta\lambda$ = 80 nm.

path, reducing the illuminated area and consequently decreasing the eye-box size. Optimizing the diffraction angle of H_T is therefore critical to prevent interference with the face and to avoid image vignetting. This optimization is closely tied to the relative positioning of H_T and H_R. Regarding the design of the collimated projector, its aperture must be configured to avoid contact with the face, which inherently limits its size. The optical path length directly correlates with the eye-box size, while the divergence angle of the projector's light determines the FOV. The dimension of H_T is also related to the projector's specifications.

In conclusion, this study has revealed the effective method for mitigating chromatic dispersion and extending eye-box in a novel dual-holographic dispersion-compensating reflective combiner structure. Moreover, the relationship between chromatic dispersion and eye-box extension has been clarified. This finding reinforces the potential of off-axis holographic reflective combiners for compact, high-performance near-eye displays. Our future research will focus on the incorporation of holographic angular multiplexing technique for further optimizing FOV and eye-box.

Funding. National Research Foundation of Korea (RS-2024-00358092); Alchemist Project MOTIE&KEIT Grant (2410005254, 20019169).

Disclosures. The authors declare no conflicts of interest.

Data availability. Data underlying the results presented in this Letter are not publicly available at this time but may be obtained from the authors upon reasonable request.

REFERENCES

1. B. C. Kress and I. Chatterjee, Nanophotonics **10**, 41 (2020).
2. J. Xiong, E.-L. Hsiang, Z. He, *et al.*, Light: Sci. Appl. **10**, 216 (2021).
3. K. Guttag, Inf. Disp. **39**, 20 (2023).
4. B. Lee, C. Yoo, and J. Jeong, Holography, Diffractive Optics, and Applications X, Proc. SPIE **11551**, 1155103 (2020).
5. B. Shin, S. I. Kim, V. Druzhin, *et al.*, Practical Holography XXXIII: Displays, Materials, and Applications, Proc. SPIE **10944**, 109440G (2019).
6. V. N. Borisov, R. A. Okun, A. E. Angervaks, *et al.*, Digital Optics for Immersive Displays II, Proc. SPIE **11350**, 113500E (2020).
7. X. Xia, F. Y. Guan, Y. Cai, *et al.*, Front. Virtual Real. **3**, 838237 (2022).
8. A. Kalinina, A. Putilin, and S. Kopenkin, Appl. Opt. **62**, D163 (2023).
9. N. Kim, Y.-L. Piao, and H.-Y. Wu, in *Holographic Materials and Optical Systems*, I. Naydenova, D. Nazarova, and T. Babeva, (eds.) (InTech, 2017).
10. J. Xiong, K. Yin, K. Li, *et al.*, Adv. Photonics Res. **2**, 2000049 (2021).
11. X. Jiang, W. Zhou, W. Dong, *et al.*, IEEE Photonics J. **16**, 7000310 (2024).
12. H. J. Jang, J. Y. Lee, G. W. Baek, *et al.*, J. Inf. Disp. **23**, 1 (2022).